Version of Record: https://www.sciencedirect.com/science/article/pii/S0034425720300584
Manuscript_86b9ed42d1b61c815d62245bab56967e

Incorporating Environmental Data in Abundance-based Algorithms for Deriving Phytoplankton Size Classes in the Atlantic Ocean

Timothy S. Moore[a,b], Christopher W. Brown[c]

[a] *University of New Hampshire, Durham NH 03824 USA*
[b] *Harbor Branch Oceanographic Institute, Fort Pierce, FL USA*
[c] *Center for Satellite Applications and Research, National Oceanic and Atmospheric Administration, College Park MD USA*

Abstract

Environmental conditions are important drivers in regulating the distribution pattern of phytoplankton composition in the world's oceans. We constructed models that predict pico-, nano- and micro-phytoplankton size classes and assessed the impact of separately including sea surface temperature (SST) and estimates of light level in the surface mixed-layer on model skill. The empirical models were trained using size classes estimated by chemotaxonomic analysis of *in situ* high performance liquid chromatography (HPLC) pigments and environmental data originating from the Atlantic Ocean. As the accuracy of transforming pigment data into quantitative size classes is crucial when constructing phytoplankton size composition (PSC) models, we also quantified the resulting differences of our and several existing PSC models when using class sizes derived from HPLC pigments by two common chemotaxonomic methods, CHEMTAX and Diagnostic Pigments (DP). Addition of the environmental variables to abundance-based models using our approach improved the skill of correctly predicting PSC, reducing the root mean square difference (RMSD) by 10 to 20% in the best cases. Addition of SST yielded the highest percentage decreases, on average, for all three size classes, with greatest improvement in microplankton and nanoplankton fractions. These models performed equal to or better than several existing abundance-based models. The improvements in model predictions, however, could be obscured by the choice of pigment method used to generate the initial PSC data set. Insufficient data is available to assess whether CHEMTAX or DP is the more appropriate chemotaxonomic method to employ when estimating PSC. Further collection and analysis of additional water samples for phytoplankton taxa and size by

Email addresses: mooret@fau.edu (Timothy S. Moore), christopher.w.brown@noaa.gov (Christopher W. Brown)

microscopic methods - including traditional microscopic cell counts and automated methods - and HPLC pigment data are required to answer this question.

Keywords: phytoplankton, remote sensing, phytoplankton size, phytoplankton functional type

---

1. Introduction

The distribution patterns of oceanic phytoplankton communities have undergone major shifts through the course of geologic time due to changes in Earth's climate, affecting various aspects of marine ecosystems on short- (1) and long-term time scales (2). Recent changes in Earth's climate are already impacting the distributions of marine organisms (3), and any changes to marine phytoplankton communities have subsequent ramifications to marine food webs and elemental cycling with feedbacks to Earth's climate ((4); (5)). Detecting phytoplankton community distributions and their changes over global space and decadal time scales is essential for understanding the complex interactions within the Earth-ocean-atmosphere system (6), all of which is necessary for assessing and planning international management efforts on climate change as the compositions of these systems respond (7).

Long-term, continuous plankton records are sparse for much of the world's oceans. While direct measurements of plankton counts exist for some regions (e.g, continuous plankton recorder data - (8)), satellite remote sensing provides the best means to monitor phytoplankton trends and patterns over the global oceans. For the past several decades, satellite remote sensing has been used to estimate the biomass and primary production in the ocean's surface layer with reasonable accuracy (9). Shifts in global phytoplankton biomass have already been observed across regions and oceanic basins from remote sensing data analysis ((10); (11); (12)).

Methods to retrieve additional characteristics of the phytoplankton community from ocean color remote sensing data have been developed over the past 20 years based on size and taxonomic class attributes. Ultimately, all of these methods use radiometry and/or bio-optical products as their primary data source. Key differences between approaches include the specific type of data used as input and the resulting output. Abundance-based methods use chlorophyll-a concentration (Chl-a) as input ((13); (14); (15); (16)), whereas optically-based approaches use fundamental inherent optical properties, such as those using spectral phytoplankton absorption ((17); (18); (19)) or particle backscattering ((20)). Output products also differ and include phytoplankton size class (PSC; e.g. (21)), phytoplankton size distribution (PSD; e.g. (22)), and phytoplankton taxonomic class (PTC;

e.g. (23)). We refer the readers to the recent reviews by (24) and (25) for detailed descriptions and classifications of these various methods and products. For another view, a phenological compilation of these algorithms were compiled by (26), highlighting commonalities and differences in the global cyclic behavior of these products.

The distribution pattern of any given phytoplankton species is a manifestation of its realized niche ((27); (28)), the habitat in which an organism lives in the presence of competition and predation. Adding information about environmental conditions to ocean color-based algorithms should therefore improve predicted PSC/PTC-type products. This concept is attractive because Chl-*a* and other ecologically relevant variables (e.g., sea surface temperature) are routinely retrieved from satellite measurements. For example, the early PSC global model of (29) segregated vertical profiles of phytoplankton size into a series of shapes based on whether the water column was stratified or mixed, directly using the mixing layer depth as a factor in predicting phytoplankton composition. (30) developed a predictive model for Phytoplankton Functional Types (PFTs) for the North Atlantic using a neural network approach based on Chl-*a*, sea surface temperature (SST) and other variables (solar irradiation, wind, geography). Similarly, (31) developed a predictive model for high latitude plankton communities using an environmentally-based neural network, and (12) developed an algorithm to predict the median size of phytoplankton from satellite data using SST and Chl-*a*.

(13) explored the use of variable model parameters as a function of optical depth, indirectly incorporating environmental impacts on size prediction. This work ultimately led to (21), where light in the mixed layer was directly used in a function for PSC model parameters. The same model form was later adapted to use SST by both (32) and (33). These three algorithms used a conceptual model that was directly linked to phytoplankton growth. The advantage of incorporating the environmental data in these models is the ability to have flexible environment-dependent parameters, as opposed to fixed parameters (e.g., (14)).

In general, derived products from these models agree on the commonly accepted distribution patterns of phytoplankton size/taxa (see (26)), but verifying their accuracy and associated uncertainties is challenging. This is due to the sparseness of phytoplankton composition data from the field, and to the difficulties in defining a universal test metric for these algorithms. In regards to the latter point, many of the algorithms are basing products as a fraction of biomass tuned or developed with regional or global data sets of pigment data determined from high performance

liquid chromatography (HPLC) using relationships between marker pigments and phytoplankton groups. Most of the studies that use marker pigment concepts for training and validation use the diagnostic pigment (DP) method originally developed by (34) and subsequently modified by others ((29); (35); (13); (36); (14)). The DP method relates ratios of pigments to derive fractional biomass for size classes and a limited number of taxanomic groups. These ratios vary in nature across taxa, photoadaptive states, and regions. These aspects are either not considered or simplified through assumptions in the DP method, as the pigment set that comprises each size fraction is fixed a priori.

CHEMTAX is another method for deriving phytoplankton composition from HPLC pigments (37). This method has the advantage of allowing pigment ratios to vary during the processing, and optimizes the ratios and class-level abundances to the observed data. This approach has not been extensively used in developing PSC/PTC-type algorithms (38), yet possibly is better suited for this application. In contrast to the DP method, CHEMTAX produces the fractional contribution of pre-defined algal taxonomic groups to Chl-*a*. From this, size fractions can be derived from the taxonomic classes, although some taxonomic classes may span one or more size ranges (e.g., diatoms) which also introduces some potential error. In any event, a characterization of size through an alternative method would likely result in a different model prediction, but so far has not been assessed.

This study has the following two objectives: (1) to evaluate how adding environmental information into PSC models impacts predictive skill relative to those solely using abundance-based estimates derived from ocean color radiometric data, and (2) to quantify the differences in PSC predictions when using different chemotaxonomic methods to derive phytoplankton size distribution from HPLC pigment data.

2. Methodology

An overview of our model development to retrieve phytoplankton size class and biomass fractions in the ocean's surface layer is shown in Figure 1. This approach blends a biomass-based model form used by (14) with model parameterization schemes introduced by (21) and (33). The suite of models in this study were constructed using an aggregated data set of coincidental phytoplankton pigment and environmental data obtained from satellite matchups. Phytoplankton size classes were derived from HPLC pigments obtained from multiple data sets restricted to the Atlantic Ocean using chemotaxonomic methods, and co-located with six satellite-derived variables. Bootstrapping was

performed to partition the data set into training and validation subsets in order to derive model parameters and uncertainties through iterative repetition with random selection. Details of the HPLC pigment, satellite-derived variables, and model development are presented in the following sections.

2.1. Pigment Data

Surface phytoplankton pigments were acquired from existing data sets of HPLC samples collected from a variety of regions in both hemispheres of the Atlantic Ocean (Table 1), including oligotrophic gyres, productive shelf waters, temperate open seas and equatorial regions (Figure 2). Data were screened for the presence of specific pigments necessary for generating size fractions (see Sections 2.3.1 and 2.3.2). A total of 1,211 surface samples from the period spanning 1997 to 2014 were available after initial quality control. A surface sample was defined as a measurement taken in the upper 30 meters. If multiple samples per station were present within this depth interval, pigment data were averaged.

This data set was further assessed for quality control to minimize outliers, particularly as they impact the model parameterizations. These checks were based on the premises that microplankton were the dominant size fraction at higher levels of biomass, and conversely were low fractions at low biomass. The following checks were used based on CHEMTAX and DP fractions: 1) at Chl-a $< 0.2\ mg/m^3$, micro fraction < 0.2; 2) at Chl-a $> 1\ mg/m^3$, micro fraction > 0.05; and 3) at Chl-a $> 1\ mg/m^3$, pico fraction < 0.1. With these checks applied, the total number of points used in the analysis was N=1083.

2.2. Satellite Data Sets and Match-ups

Surface pigments were paired with coincidental 8-day composite, gridded level-3 satellite-derived products for mixed layer depth (MLD), sea surface temperature (SST), photosynthetic available radiation (PAR), and diffuse attenuation coefficient at 490 nm (K_{d490}) (Table 2). All products were obtained freely on the internet. Briefly, PAR and K_{d490} global images were obtained from the NASA DAAC, and included SeaWiFS (1997-2010) and MODIS-Aqua (2010-2014) data products, The MLD products were obtained from the Oregon State University Primary Productivity website as 8-day composites using the 0.125 density contrast, derived from the 3-hourly HyCOM global reanalysis (model GLBu0.08). Daily Optimum Interpolation SST (OISST) data were obtained

from the NOAA (`https://www.esrl.noaa.gov/`) and averaged into 8-day composites. Spatial resolution of the satellite data ranged from 4 km^2 to 25 km^2 across the products. We used a search radius of 25 km for locating nearest pixels owing to clouds and missing information from some of the satellite data sets. All valid pixels within the 25 km of the pigment data location were subsequently averaged. We derived the average irradiance in the mixed layer (IRR_{mld}) according to the following equation:

$$IRR_{mld} = \frac{PAR}{K_{PAR} Z_m}[1 - exp(-K_{PAR} Z_m] \quad (1)$$

where Z_m is the depth of the mixed layer (equivalent to MLD), and K_{PAR} was derived from K_{d490} using the relationship developed by (39).

2.3. Predicting Phytoplankton Class Size

Phytoplankton taxa and size classes were estimated from the HPLC pigment data using both the DP and CHEMTAX methods. The two resulting phytoplankton size data sets served for parameterizing the PSC models and validating the predicted size fractions for uncertainty metrics. We summarize the salient aspects of each method below.

2.3.1. The Diagnostic Pigment Method

The DP approach converts HPLC data directly into three PSCs that are defined by traditional size ranges: pico- ($< 2\mu m$), nano- ($2\mu m < x < 20\mu m$) and microplankton ($> 20\mu m$). This is the most commonly used method for generating phytoplankton size groups from HPLC data and is based on sums and ratios of auxillary pigments that are associated with certain phytoplankton groups and associated size ranges. The central criteria of this method is assigning one (or more) diagnostic pigment to a size class, and normalizing a weighted sum (numerator) to the sum of all diagnostic pigments used across size classes (denominator). The DP method detailed in (21) was used in this study to derive size fractions and the diagnostic pigments and their associations with each PSC are described in their Table 2.

2.3.2. The CHEMTAX Method

The CHEMTAX method (37) converts HPLC to phytoplankton taxonomic composition, yielding fractions of phytoplankton abundance to the taxonomic class level present relative to overall biomass as determined by Chl-*a*. The algorithm performs a best fit analysis of the matrix of measured HPLC

pigments to pre-set phytoplankton taxa defined by an initial pigment ratio (IPR) table. Through an iterative process, the program adjusts the entries in the IPR table until a residual criterion or loop limit is met. The end result is a matrix of phytoplankton class fractions and final pigment ratios (FPR) that best approximate each entry.

CHEMTAX assumes that all samples in the phytoplankton input matrix are in a similar physiological state (37), and a single IPR table (and associated FPR table) is representative of the entire population in the matrix. Natural phytoplankton populations from diverse environments are likely not in the same physiologic state, and pigment ratios have been shown to vary with light level (e.g., (40); (41); (42)). To reduce artifacts from mixing data sets in varying physiological states, the field pigment data were sorted by source (e.g. AMT data were not mixed with other data sets), and further sub-grouped by light level (i.e., surface PAR range) and time interval. The PAR ranges used were: 0-25 mol quanta $m^2 d^{-1}$, 25-50 mol quanta $m^2 d^{-1}$, and 50-75 mol quanta $m^2 d^{-1}$. Calender month was used as the time interval. These subsets were processed as independent units by CHEMTAX with IPR tables matched to the PAR level. The three PAR-specific IPR tables were formed from multiple sources in the public literature containing pigment tables derived from the Atlantic Ocean ((43); (44); (41); (45); (46); (47) - see Appendix A).

Based on our aggregated pigment data set, the nine common pigments implemented in our CHEMTAX analysis were peridinin, butanoyloxyfucoxanthin, fucoxanthin, hexanoyloxyfucoxanthin, alloxanthin, zeaxanthin, *Chl-b*, violaxanthin and Chl-*a*. The choice of pigments were constrained by those shared across the multiple field campaigns. CHEMTAX was programmed to derive the following eight taxonomic classes: diatoms, dinoflagellates, chlorophytes, prasinophytes, prymnesiophytes, cryptophytes, cyanophytes (i.e. synechococcus) and prochlorophytes.

Phytoplankton taxonomic groups derived from CHEMTAX were assigned to size fractions comparable to those produced by the DP method. The sum of cyanophytes and prochlorophytes fractions yielded the picoplankton size class; the sum total of chlorophytes, prasinophytes, prymnesiophytes and cryptophytes fractions provided the nanoplankton; and the sume of diatoms and dinoflagellates formed the microplankton size class.

2.4. Model Development and Evaluation

PSC models were formulated and evaluated for their skill in predicting the biomass fraction of the following three phytoplankton size classe: pico-, nano- and microplankton. A logistic model was

used for both pico- and microplankton based on the form of (14). The logistic model was chosen because the sigmoid shape was best suited for the data (see 4.1). We developed and tested models without and with environmental data. The former are referred to as the *baseline* models. Our approach for the latter combined aspects of (33) and (21) to create dynamic model parameters as functions of the environment. Furthermore, separate models were constructed and assessed from each of the chemotaxonomic methods. Bootstrapping was applied for developing model parameters and performance characteristics (see 2.4.1). Performance statistics for the models of (14), (13) and (33) were also calculated using our data for comparison purposes.

The (14) model (referred to as H11 henceforth) directly produces phytoplankton size fractions (of biomass) for pico- and microplankton with Chl-a as the input variable. In (14), the pico- and microplankton models were different. Here, we use the H11 microplankton model for both pico- and microplankton defined as:

$$F_i = \frac{1}{[b_{i,1} + exp(b_{i,2} * x + b_{i,3})]} \tag{2}$$

where the subscript i equals either p (for picoplankton) or m (for microplankton), x is the log of Chl-a) and $b_{i,N}$ are parameters determined by nonlinear optimization in MATLAB. The nanoplankton fraction was derived by:

$$F_n = 1 - F_p - F_m \tag{3}$$

This constrains the fractions to sum to one, and thus any errors in pico- and microplankton models are cumulatively translated into the nanoplankton fraction.

Whereas the H11 model solves directly for fraction of biomass as a relative amount, (13) and (33) (henceforth referenced as B10 and B17, respectively) directly solve for the absolute size-fractionated Chl-a, from which the relative fraction can be derived. The B17 size models are identical in form to B10 - both solve for the amount (i.e, Chl-a) of picoplankton, and nanoplankton plus picoplankton. In these models, fractions must sum to unity. Thus, the nanoplankton and microplankton fractions are derived by subtraction. The main difference between the two models is that B17 incorporates SST as an index for the values of the model parameters.

2.4.1. Bootstrap and Binning Environmental Variables

A baseline set of parameters were derived from the full data set for both picoplankton and microplankton models. The bootstrap method (48) consisted of repeated creation of training and validation data sets using a random number generator based on a 75/25% split of data, respectively. For the baseline model that did not include environmental variables, 1000 iterations (without replacement) were run. Model parameters to the logistic functions were derived for each iteration, and averaged to obtain gross baseline parameters.

In order to incorporate external environmental conditions into the models, picoplankton and microplankton size class fractions were re-ordered by ascending environmental parameter following (21, 33). For this study, SST, PAR, and IRR_{MLD} were each independently evaluated. The logic behind this approach is that environmental links to PSC will be expressed in model parameters. Starting with the lowest value for the given environmental variable and extending to a higher value determined by a fixed window size, subsets of Chl-a and size fraction pairs were set aside for model parameterization and validation. A window size of 150 sequential data points was used, which we determined from trial and error as an optimal number for window width. The first 150 ordered points based on SST, for example, would be used for the first parameterization. On the next increment, the window would advance to the second point in that subset as the new starting point. The process was repeated until the highest value of the environmental variable was reached (a total of 637 times or intervals) for the higher end of the sliding window. At each interval along the gradient, parameters to the logistic model were derived and saved. This resulted in a set of model coefficients that were fitted to constrained ranges of environmental variables.

The re-ordering of size data from the HPLC pigments varied with environmental variable, producing three different versions of sorted data. Uncertainties for each step were computed with the a validation set within the same range as the sliding window. The process was repeated with new training and validation data created from random numbers. We ran 1000 iterations of this process, creating a large matrix of model parameter coefficients for the pico- and microplankton models and associated uncertainties. To our knowledge, this technique permits the introduction of only one environmental variable to a function at a time.

For each iteration in the bootstrap sequence, Root Mean Square Difference (RMSD) was calculated for the three size fractions derived using our baseline and environmental-based models, and the models of H11, B10 and B17. RMSD is used instead of Root Mean Square Error because an

error is the difference between an observation and the truth, which is unknown in our study. A total of 30 RMSD calculations were made per iteration (three size groups **X** five models **X** two pigment methods), and then averaged to a single RMSD values for each model and size class. RMSD was computed as follows:

$$RMSD = \sqrt{\frac{\sum_{i=1}^{n}(x_i^2 - y_i^2)}{n}} \tag{4}$$

where x_i = observed and y_i = modeled output.

3. Results

3.1. Comparison of Chemotaxonomic Methods

Despite fundamental differences in the construction of the size class fractions, the two chemotaxonomic methods generally agree (Figure 3). Mean phytoplankton size class fractions computed by CHEMTAX and DP display a positive linear relationship, indicating an underlying similarity in how the auxillary pigments are used by the two methods. On closer examination, notable differences are seen, with considerable fractional variability for any given size group. The RMSD values between the two methods are 0.11, 0.20 and 0.17 for picoplankton, nanoplankton and microplankton, respectively. The resulting picoplankton and microplankton fractions generally were slightly lower for CHEMTAX than DP, particularly at lower fractions. The nanoplankton fraction, on the other hand, was considerably higher for CHEMTAX than that generated using DP at fractions > 0.2. Without any other independent measure of size fractionation (e.g., cell counts), it is not possible to conclude which method is more accurate for this data set. Ultimately, these differences are expressed in the model parameterization. We note that PSC produced from methods based on the DP results could display similar trends. In other words, models based on DP would tend to report higher picoplankton and microplankton fractions compared to CHEMTAX derivations, with a consequent decrease in nanoplankton.

3.2. Model Form and Parameterization

The PSC models constructed in this study (collectively referred to as MB19 henceforth) for pico- and microplankton contain three parameters ($b_{i,1}$, $b_{i,2}$ and $b_{i,3}$) that govern the overall shape of the

functional response. The predicted biomass fraction for picoplankton takes the form of an inverse logistic function (sigmoid shape) with fractions decreasing with increasing chlorophyll concentration, whereas the shape of the predicted microplankton fraction is sigmoid with fraction increasing with increasing Chl-a (Figure 4). The resulting shape of the predicted fraction for nanoplankton is bell-shaped with a peak located at medium Chl-a concentrations (not shown). These baseline models, i.e. those without environmental variables, follow more closely to the B10 predictions in shape than H11, with larger relative differences seen in our models developed with the CHEMTAX data. We used a different model form for picoplankton than H11, which explains some of the shape disparity. Our baseline model systematically predicts lower microplankton fractions compared to the H11 model using the same CHEMTAX transformed data (Figure 4).

The mean and standard deviation of the model parameters for the environmental treatments (SST, IRR_{MLD} and PAR) using CHEMTAX data set from the full bootstrap process are shown in Figure 5. Parameters of both the picoplankton and microplankton models varied across the ranges of these three environmental variables, but were similar in shape for the two pigment methods for each environmental treatment (not shown). The $b_{i,1}$ parameter average exhibits the least amount of variation, and the $b_{i,2}$ parameter displaying the most. The shape of the $b_{i,3}$ parameter was generally similar to that of the $b_{i,2}$ parameter, though muted. Over the range of SST, averaged $b_{i,2}$ and $b_{i,3}$ varied over two-fold. The parameters changed slope at multiple positions along the environmental gradient for each model. For SST treatments, $b_{p,2}$ and $b_{p,3}$ in the picoplankton model changed slope at or near 13°C, 18°C and 24°C. Similar elbow points appear in the microplankton model at 10°C, 15°C, 20°C and 25°C, while $b_{m,3}$ generally showed less pronounced elbows except near 20°C and 25°C. Similar elbow points and variations were observed for the parameters over the ranges of IRR_{MLD} and PAR.

Single sets of model parameters from the smoothed average of these iterations were generated for each phytoplankton size class, environmental variable, and chemotaxonomic method. The smoothing algorithm was applied to the mean values of the parameters across each environmental range, and a look up table (LUT) was created for each parameter indexed by the environmental variable. This approach differs from B17 where functions were fit to the environmentally-dependent model parameters. For each pigment method, the RMSD values during each iteration were derived for the baseline and environmental model treatments from the validation data subsets. These were then tabulated and averaged to single, bulk statistics (Tables 5, 6).

3.3. Model Performance and Impact of Incorporating Environmental Variables

Incorporating environmental variables into our PSC models improved the average performance over their baseline versions in the majority of cases (Tables 5, 6). The only exceptions were the picoplankton models indexed by PAR and IRR_{MLD}, where including these variables yielded no significant reduction in RMSD. Addition of SST yielded the greatest improvements in average performance to all size fraction models estimated by both chemotaxonomic methods, followed by IRR_{MLD} and PAR (Tables 5, 6). The CHEMTAX and DP picoplankton fraction predictions improved with the addition of SST, with a reduction in RMSD to 0.122 (9.6%) and 0.118 (11.9%), respectively. Similarly, improvements in the models of the remaining two size fractions gained by the incorporation of SST were greater in both pigment treatments. Average RMSD of the nano- and micro-plankton models from the DP treatment decreased to 0.136 (31.0%) and 0.167 (11.6%), respectively. The CHEMTAX data set showed a greater improvement in the microplanton fraction (20.6%), and a smaller level of improvement for the nanoplankton (24.2%) relative to DP. Since the nanoplankton fractions are derived from both pico- and microplankton models, this size fraction prediction improved the most, and cumulatively benefited from gains in each size fraction models.

Among these three environmental variables, SST reduced RMSD the most overall. However, the overall pattern of improvements seen in Tables 5 and 6 suggest a degree of covariance between the environmental variables. The IRR_{MLD} is directly derived from PAR, and (33) showed a high degree of covariance between SST and IRR_{MLD} (see their Figure 1). Based on our data set, all three variables were positively correlated. The correlation was highest between PAR and IRR_{MLD} (r=0.67), and moderate between both SST and PAR (r=0.52) and SST and IRR_{MLD} (r=0.53). Thus, the patterns seen in the RMSD changes for the different environmental variables was similar owing in part to these covariations.

3.4. Comparison to Previous Abundance-based PSC Models

In general, the overall performances of the environmentally-augmented MB19 models performed better than the PSC abundance-based models that we compared (Tables 5, 6). This was not unexpected as the external models were developed using different data (though with some overlap), different pigment/size methods (i.e. CHEMTAX vs. DP method), different models, and different input variables. The baseline performances were at slightly better (picpoplankton) or roughly equal (nanoplankton and microplankton) to the same comparative models.

Detailed examination of model RMSD shows a more varied performance over the range of the environmental variables considered (Figure 6). Across the full environmental ranges, the environmentally-augmented MB19 models always had the lowest RMSD. Interestingly, the RMSD values of the baseline MB19 (without environmental variables added) were considerably higher than the other models for retrieving the microplankton fraction, and consequently the nanoplankton fraction, throughout their respective lower values, i.e. less than 15°C for SST, 10 mol quanta $m^2 d^{-1}$ for IRR_{MLD}, and 30 mol quanta $m^2 d^{-1}$ for PAR. Improvements of picoplankton retrievals relative to the baseline $MB19$ model were seen at lower (< 15°C) and higher temperature (> 20°C), with little to no change in between. For the microplankton model, larger improvements are present over the same ranges, and also show similar model performance between 15°C and 20°C.

The combined improvements of the pico- and microplankton fractions translated into the improved retrieval of the nanoplankton fraction across the temperature range except 18°C (Figure 6). The MB19 models using PAR and IRR_{MLD} show similar range-dependent improvements, with the largest overall reduction in RMSD in the nanoplankton fraction. To explore this further, we examine the model with SST parameterization as a general case applicable to the PAR and IRR_{MLD} models.

3.5. SST Model Analysis

The biomass fractions of the three size classes predicted by the SST MB19 model relative to the baseline over a range of Chl-a provide insight into how adding SST influences retrieval skill (Figure 7). The model curves in Figure 7 were separated by 10°C temperature ranges for ease of viewing. For the picoplankton size class, the MB19 SST model predicts higher fractions at higher temperatures for all but the highest Chl-a concentration. This is most evident in the 15-25°C picoplankton plot that shows the systematic increase in fraction with increasing temperature. At the highest Chl-a, i.e. $> 10\ mg/m^3$, no temperature dependency exists, although this was beyond the range of the model; predictions of biomass fraction decline to zero. In addition, an offset in the position of this systematic increase relative to the baseline (as indicated by the dashed line) shifts upward as temperatures increase, improving the retrieval of predicted fraction. For instance, the biomass fraction of picoplankton is predicted to be higher for all Chl-a levels relative to the baseline model at high temperatures (25-35°C) (Figure 7, upper left panel). For the microplankton class, the modulations in biomass fraction and its position relative to the baseline as functions of temperature

are more complex. Increasing temperature generally decreases fraction, except at temperatures ranging between 15-25°C and Chl-a between 0.3 to 3 mg/m^3 where the opposite is seen. For the nanoplankton class, the SST model generally predicts a response intermediate between the pico- and microplankton size classes. Whereas increasing temperature generally decreasing predicted fraction relative to the baseline at low to medium Chl-a levels, the reverse is seen at higher chlorophyll levels.

Figure 8 illustrates the distribution of *in situ* data and modeled (CHEMTAX-based MB19 SST) biomass fraction for the three phytoplankton size classes as a function of SST and Chl-a. The distribution of *in situ* data do not fill the entire modeled domain of these variables but are located within an envelope of SST and Chl-a ranges, as demarcated by the red dashed line. While the models can predict PSC fractions outside the bounded region, they possess a higher level of uncertainty than those within the area where data are available. Analysis of image pairs (monthly SST and Chl-a in the Atlantic Ocean bounded by 70 degrees north/south latitude) indicate slightly different patterns, but distributions are still within the bounded dashed region (not shown). While the environmental spaces outside the bounded zone likely exist, they are largely beyond the study area.

Similarities and differences between the MB19 SST models (DP- and CHEMTAX-based) and the B17 model are highlighted when mapped in the same manner (Figure 9). All models predicted high fractions of microplankton at Chl-a levels above 1 mg/m^3, yet differ on the influence of temperature: the B17 model predicts higher fractions with less sensitivity to temperature, whereas the CHEMTAX MB19 model restricts the highest fractions of microplankton to lower temperatures, with fractions decreasing as temperature increase. The MB19 model developed from DP data does not show this and appears to be more similar to the B17 predictions. The nanoplankton models all predict higher fractions in intermediate Chl-a values (0.1 mg/m^3 to 1.0 mg/m^3), although differences are also seen. The nanoplankton fractions for our models (DP and CHEMTAX) were derived from equation 3, and are thus dependent on the pico- and microplankton size models, essentially the residual difference from unity. For B17, explicit nanoplankton fractions are also derived but are not dependent on the microplankton fraction (only dependent on the picoplankton fraction). Of the predicted fields for nanoplankton, our CHEMTAX temperature-dependent prediction shows higher fractions in the intermediate Chl-a range, and also larger values over a larger SST - Chl-a space than the other two.

3.6. Application of the Models

Application of the MB19 SST models to monthly image composites derived from VIIRS for January and July 2017 yields the commonly expected distribution pattern of the three phytoplankton size classes (Figure 10). Pico- and nanoplankton size classes represent the major biomass fractions across much of the Atlantic Ocean. Comparison of the distribution pattern of these two size classes between the months also shows the expected seasonal expansion/contraction between these two fractions in the North and South Atlantic subtropical gyres. Microplankton represent only a minor fraction of phytoplankton biomass during the months shown, but their fraction increases significantly during autumn/spring months in temperate zones (not shown).

Difference maps between the MB19 baseline model and the SST model for January and July 2017 reveal systematic regions of relative positive and negative differences across the Atlantic Ocean (Figure 11). The baseline model overestimates picoplankton relative to the SST model in much of the subtropical gyres and temperate zones, and underestimates them in the equatorial region. This comes at the expense mostly of nanoplankton, which are consequently underestimated in the regions where picoplankton are overestimated. Microplankton distributions showed the smallest differences, likely because this size fraction was generally low across much of the region (Figure 10). Several interesting patterns appear in the difference maps that are coherent with oceanographic features. For example, a picoplankton/nanoplankton overestimate/underestimate feature is seen in both months that closely follows the pattern for the Gulf Stream along the U.S. southeast coast. Another feature with opposite associations is visible along the southeast coast of Canada resembling the Labrador Current. Both of these oceanographic features have strong SST expressions, and highlight the influence of SST on PSC in the model. These maps in general illustrate that most of the differences are contained in a picoplankton-nanoplankton trade-off with lesser changes in the microplankton community during these months.

4. Discussion

4.1. Phytoplankton Size Class Prediction

We set out to test whether the remotely sensed retrieval of phytoplankton size could be improved by incorporating environmental data into an abundance-based model. This is a viable approach because 1) biomass is readily measured from remote sensing, 2) several key environmental

variables that shape phytoplankton communities (directly through niche suitability and indirectly through competition and mortality factors) are also available from remote sensing, and 3) previous studies have shown this approach to be feasible. (49) investigated size distribution in relation to environment and found dependencies between light level and size, and (33) demonstrated that environmental information could be directly included into a phytoplankton size model through model parameter dependencies.

Typically, size fraction data used in these types of studies are derived indirectly according to a suite or combination of pigment concentrations that are indicators of taxonomic composition. While numerous studies have assessed size and/or taxa fractionation biomass for the DP method (e.g., (50); (29)) and CHEMTAX (e.g., (51); (52)), a comprehensive comparison of size/taxa derived from the two methods has not yet been conducted with global data sets, although analyses on regional data sets are now emerging (38). In the absence of such an analysis with in situ data in this study, we investigated the impacts and sensitivities on size models from these two alternate chemotaxonomic approaches. We also wanted to assess how adding environmental variables impacted the relative change of predictions from the various pigment methods.

In both pigment treatments (CHEMTAX and DP), addition of abiotic environmental variables to the baseline biomass-only PSC models improved the skill of correctly predicting phytoplankton size class fractions, reducing the RMSD on the order of 10 to 20% for the different variables examined in data sets from the Atlantic Ocean. SST-integrated models yielded the highest percentage RMSD decreases, on average, for all three size phytoplankton classes. Relationships between temperature and species distributions in nature have been repeatedly observed (e.g., (53); (54); (55)). Temperature has a direct effect on physiology of marine phytoplankton (e.g., dark reactions; (56)), yet its impact on size is likely the result of an accumulation of indirect effects. In this sense, temperature acts as a proxy for other ecologically important covariates and serves as a comprehensive 'catch-all' environmental parameter (57).

The improvements appear to have limits within the constraints with our tests. In our study, we explored only a few model forms and limited model parameterization to one abiotic variable dependency at a time. We examined multiple forms of logistic models for pico- and microplankton size groups. Logistic models are commonly used to model population growth (58). The best model form we found for both picoplankton and microplankton was a three-component model with a sigmoid shape and asymptotic limits, which was based on the microplankton model used

by (14). The picoplankton fractional data used in our study was better fit to a sigmoid model and was consistent with the shape found in (13), displaying asymptoptic behavior at the low and high end of the biomass spectrum. This differed from the (14) model in shape (as shown Figure 4) that exhibits exponential behavior at the biomass low and high ends. Although this model (MB19) is fundamentally different from the (13), (21) and (33) size models, the resultant model predictions are very similar. In (21) and (33), functions were fit to estimate parameter values from environmental data. Lacking smooth features amenable to functional fitting, we used Look Up Tables (LUTs) to capture the variations seen in the environmental segments. Similar to machine learning algorithms, the risk of the LUT approach is over-fitting the model to the training data and reduced accuracy for patterns outside the data domain (59). Yet, fitting a function that does not capture the parameter variations has its own set of issues, e.g. noisy parameter selection from poor function fitting. While direct comparisons with alternative methods are outside the scope of this study, there are multiple ways to represent or incorporate environmental data with statistical methods. Other studies incorporating environmental data have developed models using multivariate linear regression (e.g., (60)) and neural networks (e.g., (31)). These approaches would allow for multiple environmental variables to be incorporated simultaneously, a potential advantage over the single variable (e.g., SST) used in our study.

What, if any, linkages can be made between the temperature-dependent model coefficients and ecological associations? Logistic model parameters have been associated with aspects of population growth (e.g, growth rate, carrying capacity) when used explicitly as growth models. In our case, we are not using the function as a growth model. In the B10 and B17 models (as well as (21) and (32)), the parameters were directly linked to phytoplankton ecological attributes, such as carrying capacity. We are hesitant to ascribe physical meaning to individual parameters in our models, even though the predicted outputs from the Brewin's B10 and our models have similar shape characteristics (Figure 4). As the Brewin family of models and our models are based on different model forms and concepts, direct comparison between parameters is not meaningful. However, similarities of overall behavior of model parameters across environmental space are seen with (21) and (33), which may suggest ecological connections.

The goal in our study was to improve model prediction by directly incorporating environmental factors, not to investigate the ecological drivers for phytoplankton size determination (e.g., (49)). In other words, we focused on accurately predicting the outcome and not elucidating any causal

relationships. (21) and (32), who modeled size fraction residuals as a function of SST, noted that the behavior of predicted size fraction outputs from their model when adjusted by environment agreed with general ecological understanding. In the same context, we interpret the predictions of our models in relation to a broad view of how model predictions change in relation to varying parameters across environmental space. In our models that incorporated environmental data, the variation of parameters across environmental space are neither static nor monotonic. For example, when ordered by temperature, our model parameters show different trends (rising or falling) within specific temperature ranges (Figure 5). The first identifiable SST range with parameter change occurs from roughly 5°C to 15°C. In this range, picoplankton parameters $b_{p,2}$ and $b_{p,3}$ decreased systematically, while microplankton parameters $b_{m,2}$ and $b_{m,3}$ increased. The next range occurs from 15°C to 25°C, where these same parameters show opposite tendencies (i.e., microplankton parameters decreased). The last range is from 25°C and higher, and showed both picoplankton and microplankton parameters increasing systematically. Whatever the underlying reason, the inclusion of SST in the model helped describe the distribution of data more accurately (Figure 8). (32) noted that SST improved predictions at colder, polar regions. Our data set does not adequately represent these regions, so we cannot verify that conclusion with our analysis. Ultimately, the parameters control the behavior of the model, and we have shown how the model responds to these changes (Figure 7). While temperature may be a covarying proxy for other environmental properties, we note the these inflection points exist and only speculate that indirect ecological connections could exist, yet the connection may be with other unknown variable(s) that covary with SST.

Potential issues of incorporating environmental data into these types of algorithms exist. Primarily, analyses with the size fraction data products derived from models using the same environmental data violate data independence. Testing for physical drivers of size structure (e.g., (49), (26) and (13)) could be compromised if an environmental variable (e.g., SST) was used to estimate size structure and employed as the environmental factor. While our work is already a form of a coupling study, we acknowledge the loss of data independence with a similar type of study with our PSC models. Yet, the benefit of data independence could be outweighed by less precise PSC products. It could be argued that the gains made through improved precision are more important than potential drawbacks of losing data independence in examining physical-biological interactions, if that is an intended use of the products.

4.2. Defining Phytoplankton Community Composition

The large and growing amount of available HPLC pigment data collected globally make it an attractive and useful source of data for developing indicators of phytoplankton composition. While the HPLC methods are robust for quantifying pigments and their concentrations, the methods that transform the pigment information into phytoplankton attributes rely upon assumptions that are often violated. This is particularly true when dealing with a composite pigment data set assembled from diverse regions. These difficulties stem from the large variability of pigments across and within phytoplankton size and taxa, the broad range of sizes and size partitions for some phytoplankton taxa, and the consequent problems in the conversion of pigment concentrations and their ratios to fractions of phytoplankton sizes and/or taxa. The HPLC-based models reviewed by (24) rely on the transformation of pigments to size fractions based on the DP method originating from (34).

Our use of both CHEMTAX and DP enabled us to assess the impact of using different chemotaxonomic methods in estimating PSC group from HPLC pigments. Fundamentally, both methods rest on the same basic assumption that different pigments determine taxonomic composition and hence size of the comprising phytoplankton. One difference between the methods is that CHEMTAX produces algal classes as an output, compared to size fractions for DP analysis, although we note that DP relies on implicit assignments of specific taxa categories to size compartments. The other key difference is that CHEMTAX allows for pigment ratios to vary during iterative processing and that pigments can be shared across different classes, whereas the DP method fixes pigments to specific algal size fractions with fixed relationships. To compare PSC models from both methods, CHEMTAX class fractions were re-organized into size fractions. This introduces another source of uncertainty because not all phytoplankton from a given taxon are the same size, and exposes the key flaw in relating pigments to specific phytoplankton size ranges.

While the addition of environmental variables improved predictive skill for both pigment treatments, the improvements were smaller than the RMSD differences between the two chemotaxonomic methods themselves (Figure 3). This suggests that the basic transformation of HPLC pigments to PSC quantities (e.g., size fractions) are a critical aspect of initializing the phytoplankton community structure. It is unknown which pigment method is better, as we did not have any validation data to compare. A number of studies have evaluated size-fractionated biomass data with pigment-derived size fractions (e.g., (61); (32); (62); (63)). Phytoplankton size and taxonomic composition from the open ocean are difficult to routinely measure, and PSC algorithms are ultimately being

evaluated against community composition estimates with imperfect derivations. Thus, we cannot state with confidence which PSC algorithm or pigment method is 'better', only that incorporating environmental data did improve the models. However, the choice of pigment method is critical and impacts skill assessment for any and all bio-optical model approaches (e.g., abundance-based, IOP-based). Newer automated technologies and data sets are emerging, such as digital microscopic imaging using flow cytometric (64) and holographic (65) techniques, that can potentially serve to confirm HPLC assessments of PSC more routinely, in addition to traditional cell counting methods.

4.3. Chlorophyll-a as an Indicator of Biomass

Abundance-based PSC algorithms are appealing because estimates of Chl-a can be derived from satellite data, routinely providing Chl-a maps over spatial and temporal scales not obtainable by other means. The premise for the abundance-based approach is based on a simple and long-standing concept that Chl-a is a proxy for phytoplankton biomass. Cellular biomass is the sum of all components of which chlorophyll-a comprises only a small fraction (up to 5%) (56). Cellular carbon content is potentially a better indicator of biomass, as it is more stable than Chl-a to external conditions over short time scales (e.g., light variation), and constitutes a greater fraction of cell biomass. The Chl-a can be converted to carbon using a chlorophyll-a to carbon ratio ($Chl:C$). This ratio, which ranges from less than 0.005 to 0.1 $mgChl-a:mgC$ (66), is influenced by a variety of factors including nutrient and light history, physiological state and taxon. Thus, size fractions based on carbon is expected to be different compared to Chl-a.

Phytoplankton size or taxonomy products could be based on carbon as a measure of phytoplankton biomass if $Chl:C$ could be integrated into a biomass-based model. (67) has developed a carbon-based size product using ocean color data via particle backscattering. Similarly, a pathway exists to do this for biomass-based algorithms using CHEMTAX or DP products combined with taxon-specific $Chl:C$. The main input fields would have to be taxonomic groups in this case. We note that CHEMTAX directly produces this form of product, while with DP individual auxillary pigments must be assigned to specific taxanomic groups (e.g., (33), (15), and (14)).

To hypothetically explore first order estimates on the differences incurred in size fractions when using carbon as the biomass indicator, we converted the CHEMTAX output from fractions of $Chl-a$ to carbon using values for taxon-specific $Chl:C$ from (68). Their study demonstrated that variations in $Chl:C$ occurred between and within different algal taxonomic groups, although not

all groups were presented. We used the value for green algae for several of the CHEMTAX groups (prasinophytes, chlorophytes and cryptophytes), for example. The comparisons between pico- and microplankton fractions show non-linear trends (Figure 12). The trends show that chlorophyll-based fractions are lower than picoplankton relative to carbon-based fractions (with a mean absolute percent difference of 23%), and microplankton chlorophyll-based fractions are higher relative to carbon-based fractions (mean absolute percent difference of 55%). Assuming model fits to these fractions have the same performance as the chlorophyll-based models we developed, the implications are that microplankton fractions would be reported lower for all conditions. In this case, most of the increased fraction would be assigned to nanoplankton, as the picoplankton differences are smaller and we would expect a smaller difference between the two model predictions for picoplankton. We note that substituting DP-derived taxonomic fractions yielded similar results (not shown). A potential advantage of using CHEMTAX is that it offer an access to a wider range of taxonomic groups over DP, dependent on the pigments used and taxonomic groups known a priori. For any case, $Chl : C$ assessments of algal classes are required. While these ratios vary within classes themselves, they would provide the link from $Chl - a$ to carbon-based modeling. Whether Chl-a or carbon-based models are used, incorporating environmental data into the models would improve predictive capability for deriving phytoplankton size fractions.

5. Conclusions

Phytoplankton size models are important tools for understanding global distributions of ecological compartments (69) and refining estimates of global oceanic primary productivity (33). We chose to explore abundance-based models, one of several types, in part due to its simplistic divisions and amenability to satellite observation. We were also interested in combining other environmental data from satellites into the model, based on the influence of the abiotic environment in shaping phytoplankton communities, expressed through taxonomic and hence size distributions. Based on the models of (33) and (14), we examined the performances of phytoplankton size models with environmental-based parameters using size-partitioned data sets using two different pigment methods.

Addition of environmental variables to biomass-based models using the approach tested here improved the skill of correctly predicting PSC to varying degrees. Addition of SST yielded the highest percentage decreases on average for all three size classes: pico-, nano-, and micro-phytoplankton.

This result is logical and ecologically reasonable, as adding information about environmental factors, which are known to shape phytoplankton communities, should improve retrieval accuracy. However, and most importantly, the skill improvements were smaller than the overall differences between the two chemotaxonomic methods themselves. The basic transformation of HPLC pigments to PSC quantities is a critical step for defining the size community, and basic improvements to model prediction could be gained if it were known which pigment method was better. Insufficient data is available to unequivocally state if the DP or CHEMTAX method is better suited for estimating phytoplankton taxonomic and class size. More water samples must be collected and analyzed through microscopic methods (e.g., direct counting, flow cytometry and other automated methods) for phytoplankton size and taxonomic composition in conjunction with HPLC pigment analysis.

Acknowledgments

We thank Rob Thomas at the British Oceanographic Data Centre for providing HPLC data sets from the AMT cruises, the researchers who contributed their data to the CLIVEC and Pangea data sets, and all the researchers who contributed to NASA's SeaBASS archive. Availability and sharing data sets are essential to fundamental science and advancing the broad knowledge base. We also thank Paul DiGiacomo, Samir Chettri and Veronica Lance for facilitating the transfer of funds, and Bob Brewin and two anonymous reviewers for valuable comments and suggestions that improved a previous version of this manuscript. This study was supported and monitored by NOAA's Center for Satellite Applications and Research under Contract Number DG133E-10-CQ-0034/T0002. The views, opinions, and findings contained in this report are those of the author(s) and should not be construed as an official National Oceanic and Atmospheric Administration or U.S. Government position, policy, or decision.

References

References Cited

[1] J. M. Napp, J. G. L. Hunt, Anomalous conditions in the south-eastern Bering Sea 1997: linkages among climate, weather, ocean, and biology, Fish. Oceanogr. 10 (2001) 61–68.

[2] P. Falkowski, M. Katz, A. Knoll, A. Quigg, R. Raven, O. Schofield, F. Taylor, The evolution of modern eukaryotic phytoplankton, Science 305 (2004) 354–360. doi:10.1126/science.1095964.

[3] E. Poloczanska, M. Burrows, J. G. Molinos, B. Halpern, O. Hoegh-Guldberg, C. Kappel, P. Moore, A. Richardson, D. Schoeman, W. Sydeman, Responses of marine organisms to climate change across oceans, Frontiers in Marine Science 3. doi:10.3389/fmars.2016.00062.

[4] P. Falkowski, M. Katz, B. van Schootenbrugge, O. Schofield, A. Knoll, Why is the land green and the ocean red?, in: H. Thierstein (Ed.), Coccolithophores — from molecular processes to global impact, Springer-Verlag, Berlin, 2004.

[5] S. Tozzi, O. Schofield, P. G. Falkowski, Historical climate change and ocean turbulence as selective agents for two key phytoplankton functional groups, Marine Ecology Progress Series 274 (2004) 123–132.

[6] G. Bonan, S. Doney, Climate, ecosystems, and planetary futures: The challenge to predict life in earth system models, Science 359. doi:10.1126/science.aam8328.

[7] IPCC, Climate Change 2014: Synthesis Report. Contribution of Working Groups I, II and III to the Fifth Assessment Report of the Intergovernmental Panel on Climate Change, Geneva, Switzerland, 2014, 151 pp.

[8] A. Richardson, A. Walne, A. John, T. Jonas, J. Lindley, D. Sims, D. Stevens, M. Witt, Using continuous plankton recorder data, Progress in Oceanography 68 (2006) 27–74.

[9] C. R. McClain, G. C. Feldman, S. B. Hooker, P. Bontempi, Satellite data for ocean biology, biogeochemistry, and climate research, EOS Transactions 87 (34) (2006) 337–343.

[10] D. Antoine, A. Morel, Bridging ocean color observations of the 1980s and 2000s in search of long-term trends, Journal of Geophysical Research 110. doi:10.1029/2004JC002620.

[11] W. Gregg, N. Casey, Global and regional evaluation of the SeaWiFS chlorophyll data set, Remote Sensing of Environment 93 (2004) 463–479.

[12] J. Polovina, P. Woodworth, Declines in phytoplankton cell size in the subtropical oceans estimated from satellite remotely-sensed temperature and chlorophyll, 1998–2007, Deep-Sea Research II 77-80 (2012) 82–88. doi:10.1016/j.dsr2.2012.04.006.

[13] R. Brewin, S. Sathyendrenath, T. Hirata, S. Lavender, R. Barciela, N. Hardman-Mountford, A three-component model of phytoplankton size class for the atlantic ocean, Ecological Modelling 221 (2010) 1472–1483.

[14] T. Hirata, N. Hardman-Mountford, R. Brewin, J. Aiken, R. Barlow, K. Suzuki, T. Isada, E. Howell, T. Hashioka, M. Noguchi-Aita, Y. Ymanaka, Synoptic relationships between surface chlorophyll-a and diagnostic pigments specific to phytoplankton functional types, Biogeosciences 8 (2011) 311–327. doi:10.5194/bg-8-311-2011.

[15] M. Soppa, T. Hirata, B. Silva, T. Dinter, I. Peeken, S. Wiegmann, A. Bracher, Global retrieval of diatom abundance based on phytoplankton pigments and satellite data, Remote Sensing 6 (2014) 10089–10106. doi:10.3390/rs61010089.

[16] D. Sun, Y. Huan, Z. Qiu, C. Hu, S. Wang, Y. He, Remote-sensing estimation of phytoplankton size classes from goci satellite measurements in bohai sea and yellow sea, Journal of Geophysical Research 122 (2017) 8309–8325. doi:10.1002/2017JC013099.

[17] C. Mouw, J. Yoder, Optical determination of phytoplankton size composition from global seawifs imagery, Journal of Geophysical Research 115. doi:10.1029/2010JC006337.

[18] S. Roy, S. Sathyendrenath, H. Bouman, T. Platt, The global distribution of phytoplankton size spectrum and size classes from their light-absorption spectra derived from satellite data, Remote Sensing of Environment 139 (2013) 185–197.

[19] A. Ciotti, A. Bricaud, Retrievals of a size parameter for phytoplankton and spectral light absorption by colored detrital matter from water-leaving radiances at SeaWiFS channels in a continental shelf region off Brazil, Limnology and Oceanography Methods 4 (2006) 237–253. doi:10.4319/lom.2006.4.237.

[20] T. Kostadinov, D. Siegel, S. Maritorena, Retrieval of the particle size distribution from satellite ocean color observations, Journal of Geophysical Research 114. doi:10.1029/2009JC005303.

[21] R. Brewin, S. Sathyendrenath, T. Jackson, R. Barlow, V. Brotas, R. Airs, T. Lamont, Influence of light in the mixed-layer on the parameters of a three-component model of phytoplankton size class, Remote Sensing of Environment 168 (2015) 437–450.

[22] T. Kostadinov, D. Siegel, S. Maritorena, Global variability of phytoplankton functional types from space: assessment via the particle size distribution, Biogeosciences 7 (2011) 3239–3257. doi:10.5194/bg-7-3239-2010.

[23] S. Alvain, C. Moulin, Y. Dandonneau, F. Breon, Remote sensing of phytoplankton groups in case 1 waters from global SeaWiFS imagery, Deep-Sea Research II 52 (2005) 1989–2004.

[24] C. Mouw, N. Hardman-Mountford, S. Alvain, A. Bracher, R. Brewin, A. Bricaud, A. Ciotti, E. Devred, A. Fujiwara, T. Hirata, T. Hirawake, T. Kostadinov, S. Roy, J. Uitz, A consumer's guide to satellite remote sensing of multiple phytoplankton groups in the global ocean, Frontiers in Marine Science 4. doi:10.3389/fmars.2017.00041.

[25] IOCCG, Phytoplankton functional types from space, reports of the International Ocean-Colour Coordinating Group, No. 15 (2014).

[26] T. Kostadinov, A. Cabbre, H. Vedantham, I. Marinov, A. Bracher, R. Brewin, A. Bricaud, T. Hirata, T. Hirawake, N. Harman-Mountford, C. Mouw, S. Roy, J. Uitz, Inter-comparison of phytoplankton functional type phenology metrics derived from ocean color algorithms and earth system models, Remote Sensing of Environment 190 (2017) 162–177. doi:10.1016/j.rse.2016.11.014.

[27] G. Hutchinson, A Treatise on Limnology, Vol. II, Wiley, New York, 1967.

[28] E. Litchman, C. Klausmeier, Trait based community ecology of phytoplankton, Annu. Rev. Ecol. Evol. Syst 39 (2008) 615–639. doi:10.1146/annurev.ecolsys.39.110707.173549.

[29] J. Uitz, H. Claustre, A. Morel, S. Hooker, Vertical distribution of phytoplankton communities in open ocean: An assessment based on surface chlorophyll, Journal of Geophysical Research 111. doi:doi:10.1029/2005JC003207.

[30] D. Raitsos, S. Lavender, C. Maravelias, J. Haralambous, A. Richardson, P. Reid, Identifying four phytoplankton functional types from space: An ecological approach, Limnology and Oceanography 53 (2008) 605–613.

[31] A. Palacz, M. S. John, R. Brewin, T. Hirata, W. Gregg, Distribution of phytoplankton functional types in high-nitrate, low-chlorophyll waters in a new diagnostic ecological indicator model, Biogeosciences 10 (2013) 7553–7574. doi:10.5194/bg-10-7553-2013.

[32] B. Ward, Temperature-correlated changes in phytoplankton community structure are restricted to polar waters, PloS ONE 10. doi:10.1371/journal.pone.0135581.

[33] R. Brewin, S. Ciavatta, S. Sathyendrenath, T. Jackson, G. Tilstone, K. Curran, R. Airs, D. Cummings, V. Brotas, E. Organelli, G. DallÓlmo, D. Raitsos, Uncertainty in ocean-color estimates of chlorophyll for phytoplankton groups, Frontiers in Marine Science 4. doi:10.3389/fmars.2017.00104.

[34] F. Vidussi, H. Claustre, B. Manca, A. Luchetta, J.-C. Marty, Phytoplankton in the subtropical atlantic ocean: towards a better assessment of biomass and composition, Journal of Geophysical Research 106 (2001) 19939–19956.

[35] T. Hirata, J. Aiken, N. Hardman-Mountford, T. Smythe, R. Barlow, An absorption model to determine phytoplankton size classes from satellite ocean colour, Remote Sensing of Environment 112 (2008) 3153–3159. doi:10.1016/j.rse.2008.03.011.

[36] E. Devred, S. Sathyendrenath, V. Stuart, T. Platt, A three component classification of phytoplankton absorption spectra: Applications to ocean-colour data, Remote Sensing of Environment 115 (2011) 2255–2266. doi:10.1016/j.rse.2011.04.025.

[37] M. Mackey, D. Mackey, H. Higgins, S. Wright, Chemtax - a program for estimating class abundances from chemical markers: application to hplc measurements of phytoplankton, Marine Ecology Progress Series 144 (1996) 265–283.

[38] S. Nunes, G. Perez, M. Latasa, M. Zamanillo, M. Delgado, E. Ortega-Retuerta, M. C, R. Simo, M. Estrada, Size fractionation, chemotaxonomic groups and bio-optical properties of phytoplankton along a transect from the Mediterranean Sea to the SW Atlantic Ocean, Scientia Marina 8. doi:10.3989/scimar.04866.10A.

[39] A. Morel, Y. Huot, B. Gentili, P. Werdell, S. Hooker, B. Franz, Examining the consistency of products derived from various ocean color sensors in open ocean (case 1) waters in the perspective of a multi-sensor approach, Remote Sensing of Environment 111 (2007) 69–88. doi:10.1016/j.rse.2007.03.012.

[40] J.-P. Descy, H. Sarmento, H. Higgins, Variability of phytoplankton pigment ratios across aquatic environments, European Journal of Phycology 44 (2009) 319–330.

[41] L. Schluter, L. Lauridsen, G. Krogh, T. Jorgenson, Identification and quantification of phytoplankton groups in lakes using new pigment ratios – a comparison between pigment analysis by hplc and microscopy, Freshwater Biology 51 (2006) 1474–1485. doi:10.1111/j.1365-2427.2006.01582.x.

[42] L. Schluter, F. Mohlenberg, H. Havskum, S. Larsen, The use of phytoplankton pigments for identifying and quantifying phytoplankton groups in coastal areas: testing the influence of light and nutrients on pigment/chlorophyll a ratios, Marine Ecology Progress Series 192 (2000) 49–63.

[43] M. Veldhuis, G. Kraay, Phytoplankton in the subtropical atlantic ocean: towards a better assessment of biomass and composition, Deep Sea Research I 51 (2004) 507–530.

[44] P. Goela, S. Danchenko, J. Icely, L. Lubian, S. Cristina, A. Newton, Using chemtax to evaluate seasonal and interannual dynamics of the phytoplankton community off the south-west coast of portugal, Estuarine, Coastal and Shelf Science 151 (2014) 112–123.

[45] W. H. van De Poll, D. S. Maat, P. Fischer, P. D. Rozema, O. B. Daly, S. Koppelle, R. J. W. Visser, A. G. J. Buma, Atlantic advection driven changes in glacial meltwater: Effects on phytoplankton chlorophyll-a and taxonomic composition in kongsfjorden, spitsbergen, Frontiers in Marine Science 3 (2016) 200. doi:10.3389/fmars.2016.00200.
URL https://www.frontiersin.org/article/10.3389/fmars.2016.00200

[46] X. Irigoien, B. Meyer, R. Harris, D. Harbour, Using hplc pigment analysis to investigate phytoplankton taxonomy: the importance of knowing your species, Helgoland Marine Research 58 (2004) 77–82. doi:10.1007/s10152-004-0171-9.

[47] P. Henriksen, B. Riemann, H. Kaas, H. M. Sorensen, H. L. Sorensen, Effects of nutrient-limitation and irradiance on marine phytoplankton pigments, Journal of Plankton Research 24 (9) (2002) 835–858.

[48] B. Efron, Bootstrap methods: another look at the jackknife, The Annals of Statistics 7 (1979) 1–26. doi:10.1214/aos/1176344552.

[49] C. Mouw, A. Ciochetta, J. Yoder, A satellite assessment of environmental controls of phytoplankton community size structure, Global Biogeochemical Cycles 33 (2019) 540–558. doi:10.1029/2018GB006118.

[50] R. Brewin, S. Sathyendrenath, P. Lange, G. Tilstone, Comparison oftwo methods to derive the size-structure of natural populations of phytoplankton, Deep-Sea Research I 85 (2014) 72–79.

[51] C. Llewellyn, J. Fishwick, J. Blackford, Phytoplankton community assemblage in the English Channel: a comparison using chlorophyll a derived from HPLC-CHEMTAX and carbon derived from microscopy cell counts, Journal of Plankton Research 27 (2005) 103–119.

[52] D. Mackey, J. Blanchot, H. Higgins, J. Neveux, Phytoplankton abundances and community structure in the equatorial Pacific, Deep Sea Research II 49 (2002) 2561–2582.

[53] R. D. Stuart-Smith, G. J. Edgar, A. E. Bates, Thermal limits to the geographic distributions of shallow-water marine species, Nature Ecology & Evolution 1 (2017) 1846–1852.

[54] E. Jeffree, C. Jeffree, Temperature and the biogeographical distributions of species, Functional Ecology 8 (1994) 640–650.

[55] M. L. Pinsky, G. Reygondeau, R. Caddell, J. Palacios-Abrantes, J. Spijkers, W. W. L. Cheung, Preparing ocean governance for species on the move, Science 360 (6394) (2018) 1189–1191. arXiv:http://science.sciencemag.org/content/360/6394/1189.full.pdf, doi:10.1126/science.aat2360.
URL http://science.sciencemag.org/content/360/6394/1189

[56] R. Geider, H. MacIntyre, T. Kana, Dynamic model of phytoplankton growth and acclimation: responses of the balanced growth rate and the chlorophyll a:carbon ratio to light, nutrient-limitation and temperature, Marine Ecology Progress Series 148 (1997) 187–200.

[57] H. Bouman, T. Platt, S. Sathyendrenath, W. Li, V. Stuart, C. Fuentes-Yaco, H. Maass, E. Horne, O. Ulloa, V. Lutz, M. Kyewalyanga, Temperature as indicator of optical properties and community structure of marine phytoplankton: implications for remote sensing, Marine Ecology Progress Series 258 (2003) 19–30.

[58] A. Tsoularis, Analysis of logistic growth models, Research Letters in the Information and Mathematical Sciences 2 (2001) 23–46.

[59] R. Baker, J.-M. Pena, J. Jayamohan, A. Jerusalem, Mechanistic models versus machine learning, a fight worth fighting for the biological community?, Biological Letters 14 (2018) 20170660. doi:10.1098/rsbl.2017.0660.

[60] C. Kruk, E. Peeters, E. V. Nes, V. Huszar, L. Costa, M. Scheffer, Phytoplankton community composition can be predicted best in terms of morphological groups, Limnology and Oceanography 56 (2011) 110–118. doi:10.4319/lo.2011.56.1.0110.

[61] R. Brewin, X. Moran, D. Raitsos, J. Gittings, M. Calleja, M. Viegas, M. Ansari, N. Al-Otaibi, T. Huete-Stauffer, I. Hoteit, Factors regulating the relationship between total and size-fractionated chlorophyll-a in coastal waters of the red sea, Frontiers in Microbiology 10 (2019) 1964. doi:10.3389/fmicb.2019.01964.

[62] V. Brotas, R. Brewin, C. Sa, A. Brito, A. Silva, C. Mendes, T. Diniz, M. Kaufmann, G. Tarran, S. Groom, T. Platt, S. Sathyendrenath, Deriving phytoplankton size classes from satellite data: Validation along a trophic gradient in the eastern atlantic ocean, Remote Sensing of Environment 134 (2013) 66–77. doi:doi:10.1111/j.1365-2427.2006.01582.x.

[63] J. Uitz, H. Claustre, A. Morel, S. Hooker, A phytoplankton class-specific primary production model applied to the kerguelen islands region (southern ocean), Deep-Sea Research II 56 (2009) 541–560. doi:10.1016/j.dsr.2008.11.006.

[64] R. Olsen, H. Sosik, A submersible imaging-in-flow instrument to analyze nano- and microplankton: Imaging flowcytobot, Limnology and Oceanography: Methods 5 (2007) 195–203. doi:10.4319/lom.2007.5.195.

[65] M. Twardowski, J. Sullivan, F. Dalgeish, Novel technologies to study undisturbed particle fields in the ocean, Sea Technology 57 (2016) 15–19.

[66] J. Cloern, C. Grenz, L. Vidergar-Lucas, An empirical model of the phytoplankton chlorophyll:carbon ratio - the conversion factor between productivity and growth rate, Limnology and Oceanography 40 (1995) 1313–1321.

[67] T. Kostadinov, S. Milutinovic, I. Marinov, A. Cabbre, Carbon-based phytoplankton size classes retrieved via ocean color estimates of the particle size distribution, Ocean Sciences 12 (2016) 561–575. doi:10.5194/os-12-561-2016.

[68] S. Sathyendrenath, V. Stuart, A. Nair, K. Oka, T. Nakane, H. Bouman, M.-H. Forget, H. Maass, T. Platt, Carbon-to-chlorophyll ratio and growth rate of phytoplankton in the sea, Marine Ecology Progress Series 383 (2009) 73–84. doi:10.3354/meps07998.

[69] A. Longhurst, Seasonal cycles of pelagic production and consumption, Prog. Oceanogr. 36 (1995) 77–167.

6. Tables

Table 1: Source and number of High Performance Liquid Chromotography (HPLC) samples used in this study.

Source	**Time Frame**	**N**	**N** QC'd
AMT	Aug 1997 - Nov 2010	543	498
Pangea	Feb 1998 - Apr 2007	98	82
GulfofMaine	Jan 2006 - Dec 2009	76	69
CLIVEC	Aug 2009 - Aug 2012	441	425
SeaBASS	Feb 2001 - Nov 2010	53	9
Total		1211	1083

Table 2: Name and characteristics of satellite data sets used in this study

Parameter	**Source**	**Time Frame**	Spatial Resolution	Temporal Resolution
SST	NOAA AVHRR	1997-2014	4km	8-day
PAR	NASA SeaWiFS	1997-2010	9km	8-day
PAR	NASA MODIS-Aqua	2010-2014	4km	8-day
MLD	HyCOM	1997-2014	9km	8-day
$Chl-a$	NASA SeaWiFS	1997-2010	9km	8-day
$Chl-a$	NASA MODIS-Aqua	2010-2014	4km	8-day

Table 3: Correlation coefficients between environmental variables

Parameters	**All**	**Pico**	**Nano**	**Micro**
SST/IRR_{MLD}	0.5625	0.1328	0.6032	0.6978
SST/PAR	0.5133	0.1015	0.4968	0.6207
IRR_{MLD}/PAR	0.6715	0.5457	0.7088	0.8090

Table 4: Baseline coefficients of the phytoplankton class size (PSC) models developed in this study

Size derivation	**Size fraction**	$b_{i,1}$	$b_{i,2}$	$b_{i,3}$
$CHEMTAX$	Picoplankton	1.54	5.23	3.39
	Microplankton	1.88	-3.59	0.06
DP	Picoplankton	1.41	2.82	1.72
	Microplankton	0.82	-1.33	0.39

Table 5: Root Mean Square Error (RMSD) of PSC models evaluated in this study using phytoplankton sizes classes derived from HPLC data by CHEMTAX.

Size Fraction	Test Scenarios									Existing Algorithms		
	SST	Baseline	%Change	IRR_{MLD}	Baseline	%Change	PAR	Baseline	%Change	$H11$	$B10$	$B17$
Picoplankton	0.122	0.135	-9.6	0.134	0.132	1.5	0.140	0.139	0.0	0.191	0.160	0.153
Nanoplankton	0.175	0.231	-24.2	0.189	0.229	-17.7	0.196	0.227	-13.7	0.253	0.256	0.266
Microplankton	0.150	0.189	-20.6	0.153	0.191	-19.9	0.157	0.189	-16.9	0.185	0.173	0.185

Table 6: Same as Table 4, but using phytoplankton size classes derived from HPLC data by the Diagnostic Pigment method.

Size Fraction	Test Scenarios									Existing Algorithms		
	SST	Baseline	%Change	IRR_{MLD}	Baseline	%Change	PAR	Baseline	%Change	$H11$	$B10$	$B17$
Picoplankton	0.118	0.134	-11.9	0.132	0.132	0.0	0.139	0.139	0.0	0.160	0.136	0.136
Nanoplankton	0.136	0.197	-31.0	0.147	0.196	-25.0	0.157	0.196	-19.9	0.184	0.138	0.146
Microplankton	0.167	0.189	-11.6	0.162	0.190	-14.7	0.167	0.188	-11.2	0.185	0.173	0.185

7. Figures

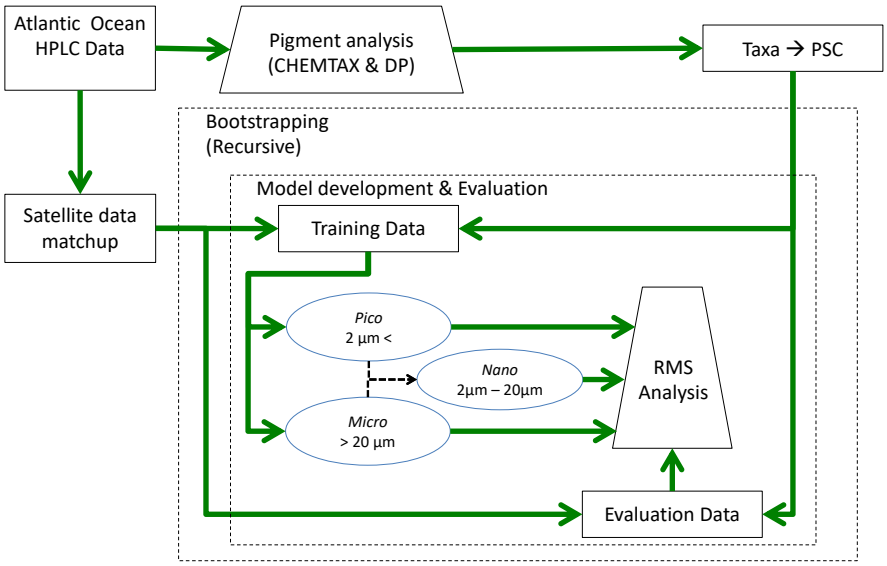

Figure 1: Schematic flow of methodological approach.

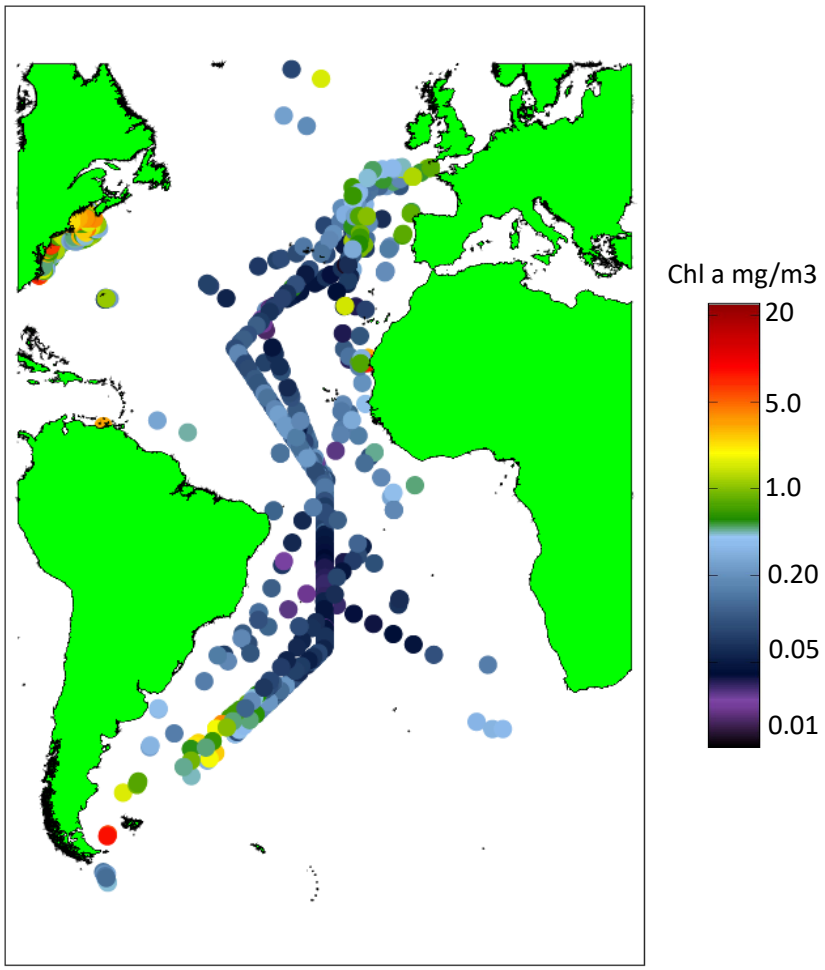

Figure 2: Map of station locations color-coded by chlorophyll-a concentration.

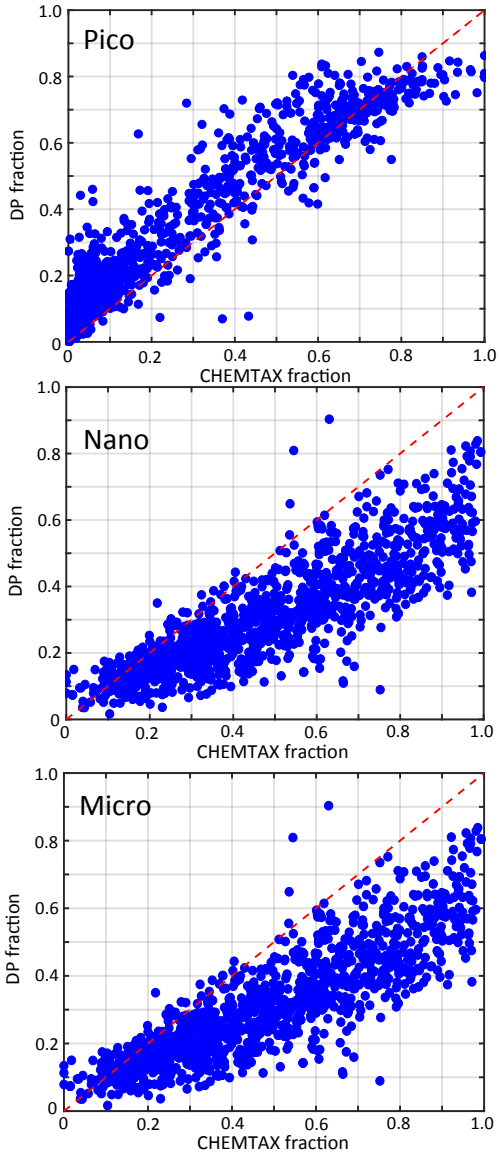

Figure 3: Comparison of phytoplankton size classes derived from CHEMTAX and the Diagnostic Pigment (DP) method. The 1:1 line is included in each plot. The data set consists of surface HPLC samples from the Atlantic Ocean (N=1083).

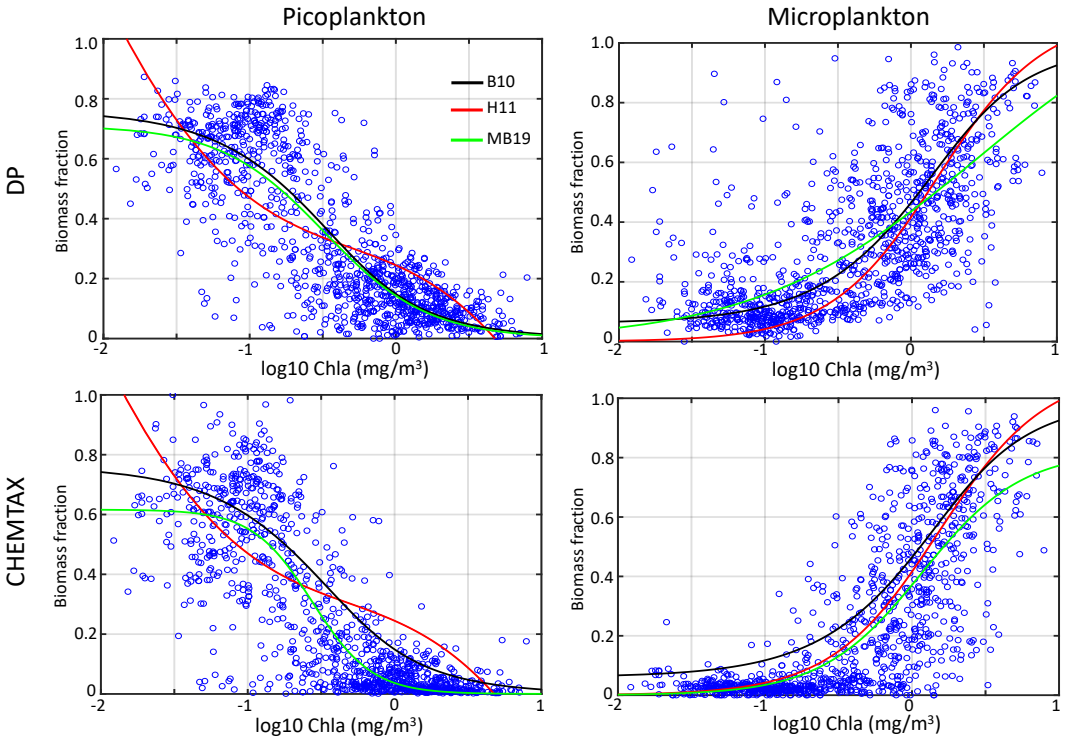

Figure 4: Baseline model fits to CHEMTAX and DP derived size fractions for picoplankton and microplankton of our models (MB19; green line). Black and red lines represent results derived by applying the data to the models of (13) and (14), respectively.

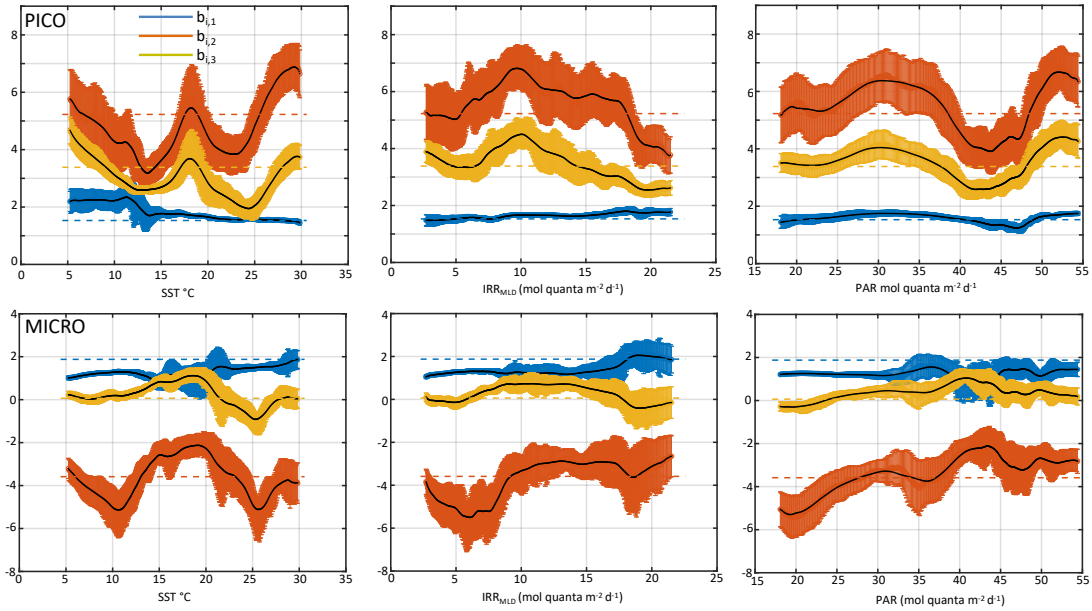

Figure 5: Mean and standard deviation of parameters across environmental space of sea surface temperature, average irradiance in the mixed layer, and photosynthetically available radiation for picoplankton (top row) and microplankton (bottom row) size class fraction models developed in this study. No nanoplankton model data are displayed because none were constructed; the fraction of nanoplankton were derived according to equation 3.

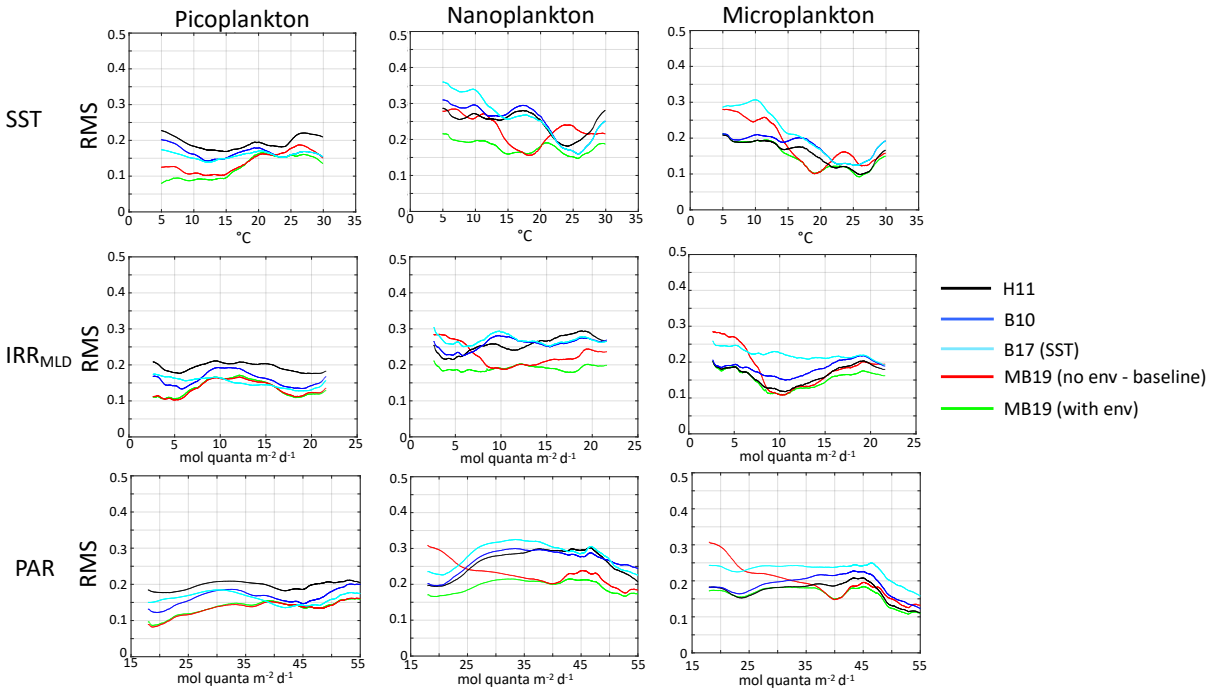

Figure 6: RMSD distributions for each PSC model across ordered environmental space.

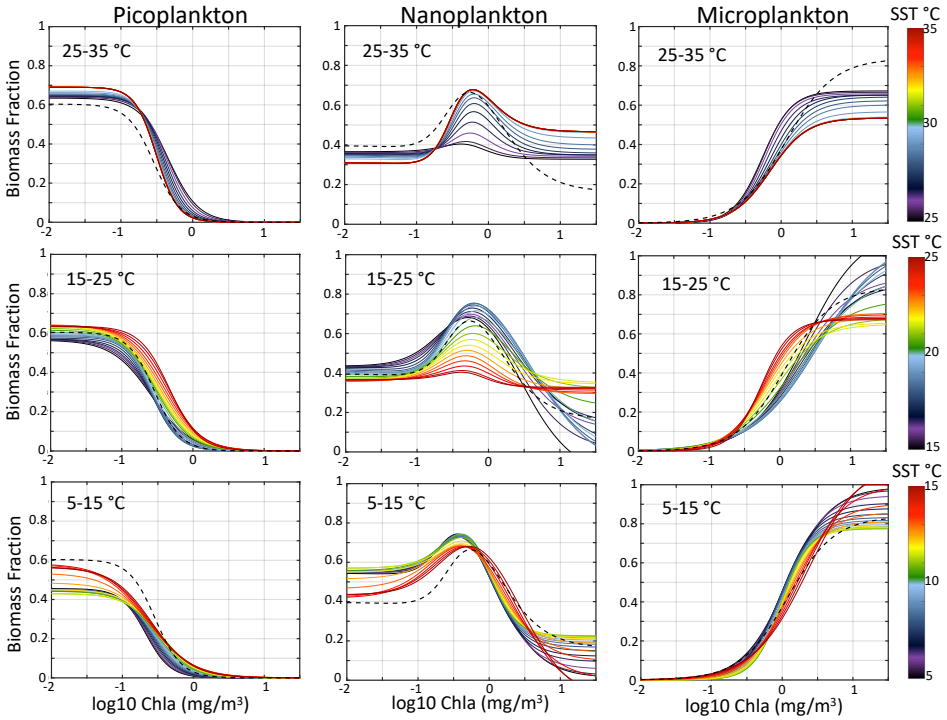

Figure 7: Predicted curves for biomass fractions of pico-, nano- and micro-plankton size classes using the sea surface temperature (SST) model developed in this study. Top row: curves in the SST range of 25 to 35°C; Middle row: curves in the SST range of 15 to 25°C; Bottom row: curves in the SST range 5 to 15°C. Black dashed line represents the baseline prediction. Note the scale change for the difference temperature ranges.

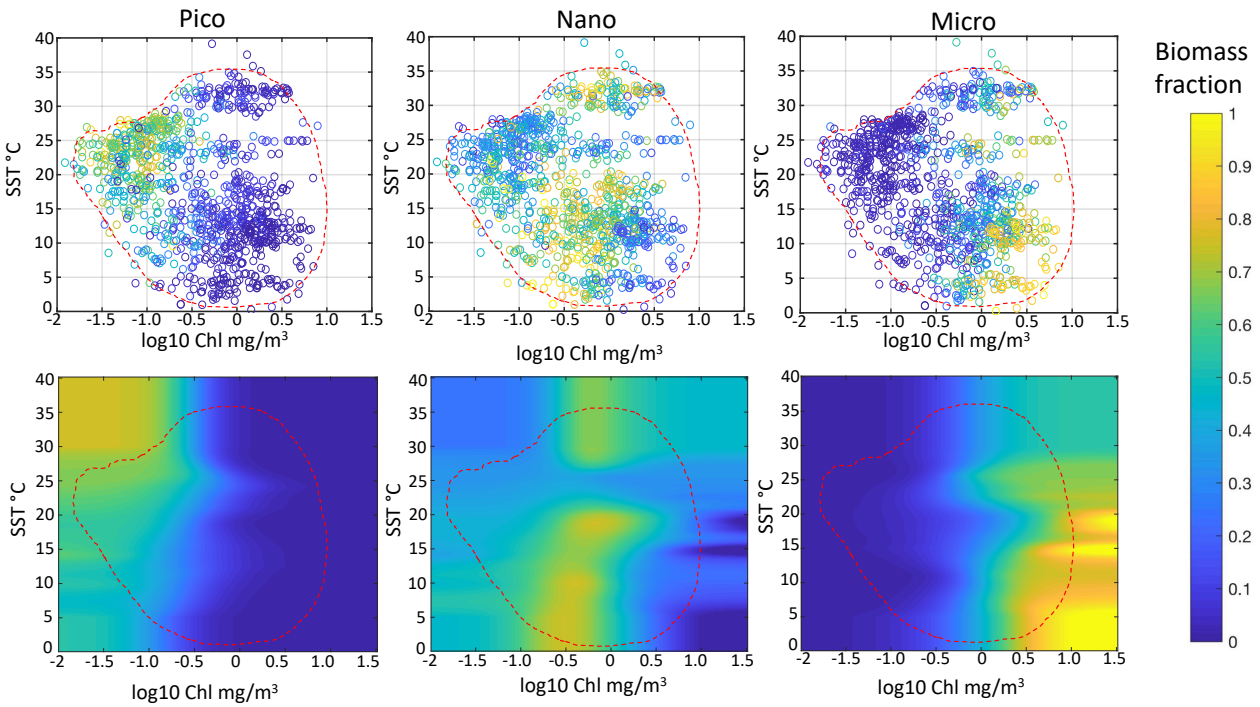

Figure 8: Distribution of *in situ* (top row) biomass fraction for pico-, nano- and micro-plankton size classes in relation to sea surface temperature (SST) and chlorophyll concentration. Points are color-coded by the intensity of the biomass fraction for the given size group. Bottom row: the same axes as the top row, with the colors expressing the size fraction intensity resulting from the MB19 model with SST. The *in situ* data distribution boundaries derived from the top row are superimposed over these plots.

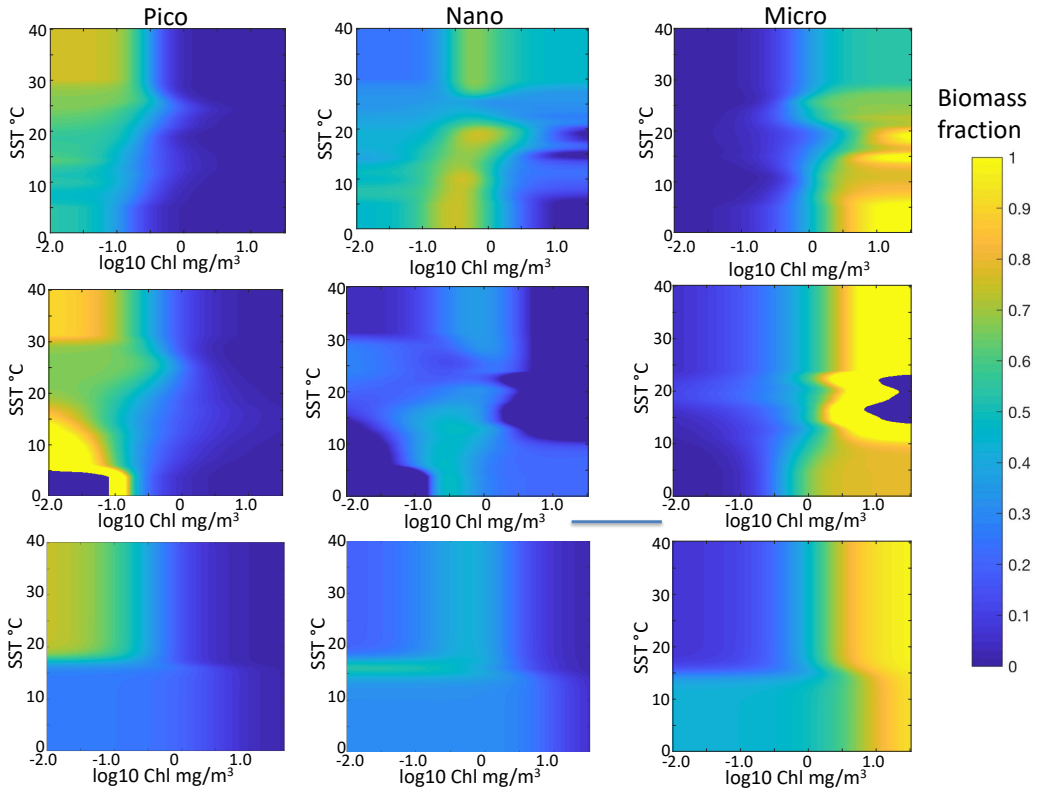

Figure 9: Distribution of biomass fraction for pico-, nano- and micro-plankton size classes (PSC) in relation to sea surface temperature (SST) and chlorophyll concentration Chl-a in the MB19 model with SST based on CHEMTAX PSC (top row), MB19 model with SST based on Diagnostic Pigment PSC (middle row), and Brewin et al., 2017 model (bottow row).

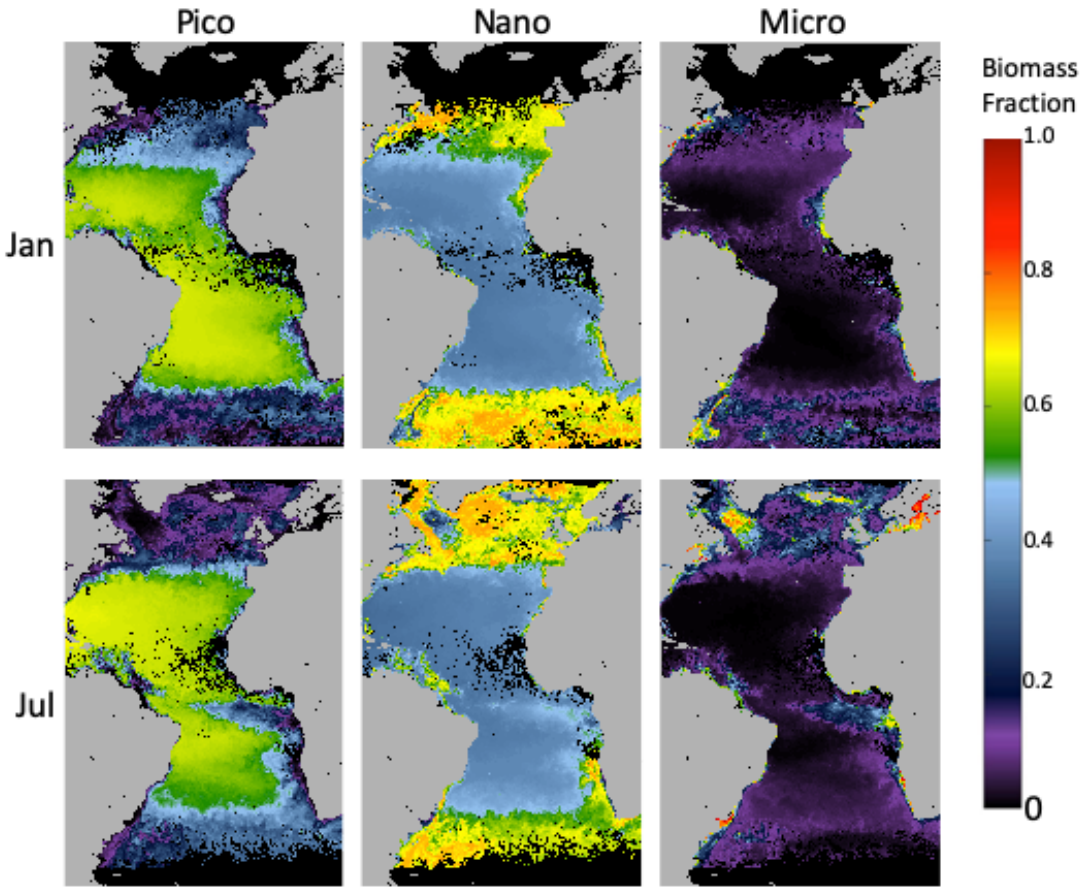

Figure 10: Distribution pattern of biomass fractions of the three size classes predicted for January and July 2017 using the sea surface temperature augmented model developed in this study.

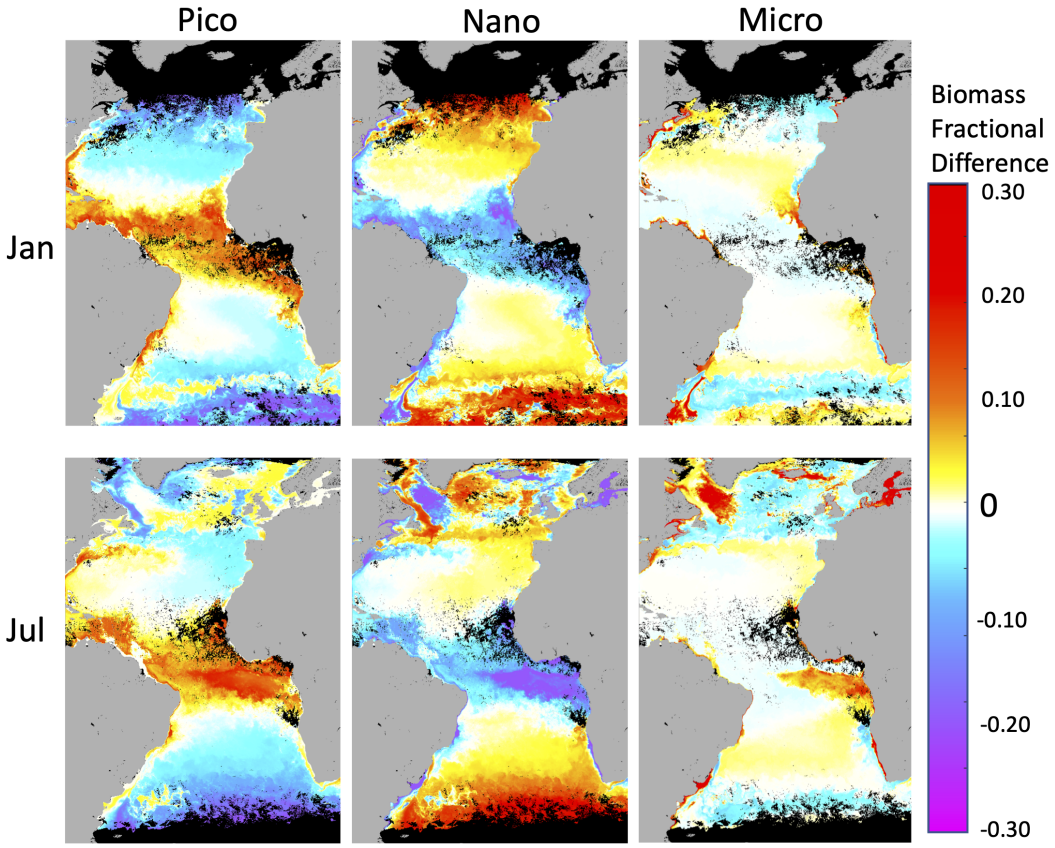

Figure 11: Difference maps between MB19 baseline model (without environment) and the MB19 model with SST for monthly VIIRS image pairs shown in Figure 10. Hotter color (reds) indicate higher SST model fractions relative to the baseline model. Black indicates regions where PSC fractions were not calculated.

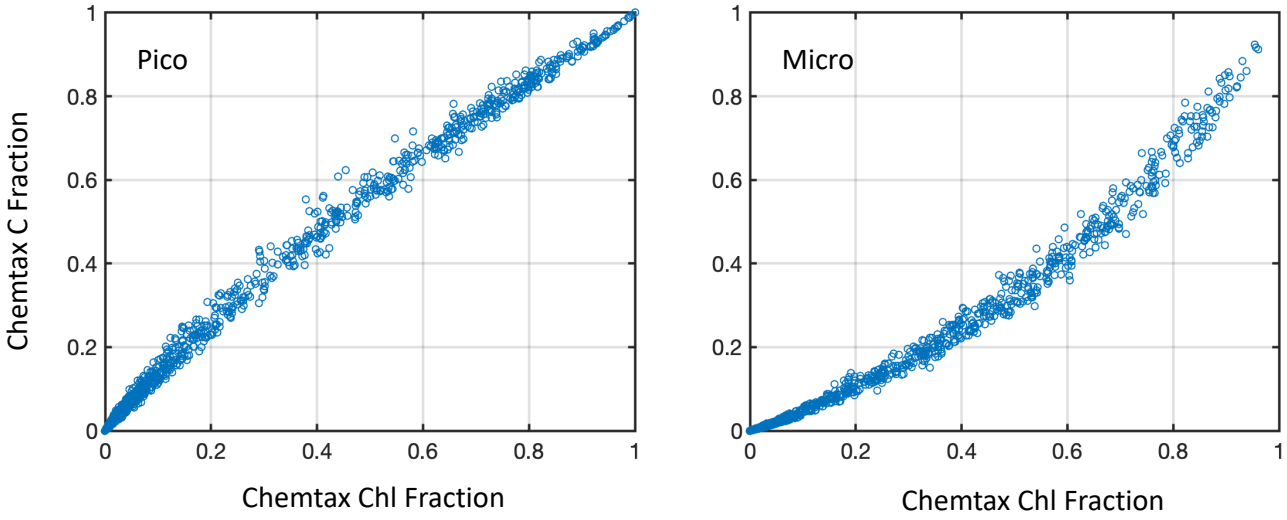

Figure 12: Carbon vs. chlorophyll estimated biomass fraction for picoplankton (left) and microplankton (right).

Appendix

Table 7: CHEMTAX Initial Pirgment Ratio table - Low PAR

Algal class	Pigment ratios								
	$Perid$	$19-but$	$Fuco$	$19-hex$	$Allo$	Zea	$Chl-b$	$Viola$	$D.Chl-a$
$Diatoms$	0	0	0.54	0	0	0	0	0	0
$Dinoflagellates$	1.06	0	0	0	0	0	0	0	0
$Cyanophytes$	0	0	0	0	0	0.49	0	0	0
$Prymnesiophytes$	0	0.3	0.43	0	0	0	0	0	0
$Chlorophytes$	0	0	0	0	0	0	0.41	0.06	0
$Prasinophytes$	0	0	0	0	0	0	0.79	0.03	0
$Cryptophytes$	0	0	0	0	0.21	0	0	0	0
$Chrysophytes$	0	0.45	0.34	0	0	0	0	0	0
$Prochlorococcus$	0	0	0	0	0	0.89	1.1	0	1

Table 8: CHEMTAX Initial Pirgment Ratio table - Medium PAR

Algal class	Pigment ratios								
	$Perid$	$19-but$	$Fuco$	$19-hex$	$Allo$	Zea	$Chl-b$	$Viola$	$D.Chl-a$
$Diatoms$	0	0	0.50	0	0	0	0	0	0
$Dinoflagellates$	1.0	0	0	0	0	0	0	0	0
$Cyanophytes$	0	0	0	0	0	0.49	0	0	0
$Prymnesiophytes$	0	0.3	0.43	0	0	0	0	0	0
$Chlorophytes$	0	0	0	0	0	0	0.41	0.06	0
$Prasinophytes$	0	0	0	0	0	0	0.66	0.03	0
$Cryptophytes$	0	0	0	0	0.27	0	0	0	0
$Chrysophytes$	0	0.43	0.62	0	0	0	0	0	0
$Prochlorococcus$	0	0	0	0	0	0.89	0.60	0	1.0

Table 9: CHEMTAX Initial Pirgment Ratio table - High PAR

Algal class	Pigment ratios								
	$Perid$	$19-but$	$Fuco$	$19-hex$	$Allo$	Zea	$Chl-b$	$Viola$	$D.Chl-a$
$Diatoms$	0	0	0.45	0	0	0	0	0	0
$Dinoflagellates$	1.0	0	0	0	0	0	0	0	0
$Cyanophytes$	0	0	0	0	0	0.49	0	0	0
$Prymnesiophytes$	0	0.30	0.43	0	0	0	0	0	0
$Chlorophytes$	0	0	0	0	0	0.10	0.41	0.06	0
$Prasinophytes$	0	0	0	0	0	0	0.53	0.04	0
$Cryptophytes$	0	0	0	0	0.21	0	0	0	0
$Chrysophytes$	0	0.45	0.34	0	0	0	0	0	0
$Prochlorococcus$	0	0	0	0	0	0.89	0.17	0	1.0